INTERNATIONAL JOURNAL FOR NUMERICAL METHODS IN ENGINEERING
Int. J. Numer. Meth. Engng 2010; **81**:537–563
Published online 5 August 2009 in Wiley InterScience (www.interscience.wiley.com). DOI: 10.1002/nme.2694

Coarse-graining of multiscale crack propagation

Ted Belytschko*, †, ‡ and Jeong-Hoon Song§

Department of Mechanical Engineering, Northwestern University, 2145 Sheridan Road, Evanston, IL 60208-3111, U.S.A.

SUMMARY

A method for coarse graining of microcrack growth to the macroscale through the multiscale aggregating discontinuity (MAD) method is further developed. Three new features are: (1) methods for treating nucleating cracks, (2) the linking of the micro unit cell with the macroelement by the hourglass mode, and (3) methods for recovering macrocracks with variable crack opening. Unlike in the original MAD method, ellipticity is not retained at the macroscale in the bulk material, but we show that the element stiffness of the bulk material is positive definite. Several examples with comparisons with direct numerical simulations are given to demonstrate the effectiveness of the method. Copyright © 2009 John Wiley & Sons, Ltd.

Received 6 December 2008; Revised 1 June 2009; Accepted 3 June 2009

KEY WORDS: multiscale; fracture; discontinuity; finite elements; extended finite element method

1. INTRODUCTION

The coarse graining of failure is a key goal in the multiscale analysis of solids. Coarse-graining of pre-failure behavior is already understood: it is the topic of a highly developed field called homogenization, see for example the monograph of Zohdi and Wriggers [1] for a general description. However, in contrast to coarse graining in the pre-failure regime, coarse graining of failure is an open topic because failure is associated with loss of material stability, which ushers in a host of numerical challenges. For example, in equilibrium processes with rate-independent materials, when the material fails at the macroscale, the partial differential equation (PDE) loses ellipticity

*Correspondence to: Ted Belytschko, Department of Mechanical Engineering, Northwestern University, 2145 Sheridan Road, Evanston, IL 60208-3111, U.S.A.
†E-mail: tedbelytschko@northwestern.edu
‡Walter P. Murphy Professor.
§Postdoctoral Fellow.

Contract/grant sponsor: Army Office of Scientific Research; contract/grant number: W911-NF-08-1-0212
Contract/grant sponsor: Office of Naval Research; contract/grant numbers: N00014-08-1-1191, N00014-06-1-0380

and the problem becomes ill-posed, see for example, Rudnicki and Rice [2] and Belytschko *et al.* [3]. In Bazant and Belytschko [4], it was shown that this leads to a solution with an infinite strain on a set of measure zero at the point where material stability has been lost. Loss of material stability can occur due to strain softening or nonassociated material laws, see Rudnicki and Rice [2] for the latter. For the dynamic field equations, material failure results in the loss of hyperbolicity of the governing PDEs, which also leads to ill posedness. For the equilibrium equations, loss of material stability results in loss of ellipticity. Therefore, a simplistic coarse-graining process where the stress–strain response that is computed at the microscale is simply passed to the macroscale is doomed to failure (of a different kind). Assumptions that are central to homogenization theory, such as periodicity and separation of length scales, are no longer applicable.

In the following, we will only refer to loss of ellipticity or material instability; by this we tacitly mean loss of ellipticity in equilibrium problems, loss of hyperbolicity in dynamic problems.

This difficulty is particularly challenging in multiscale analysis, for when a macromodel is linked with a micromodel, it is not clear how a decreasing stress due to damage and other failure mechanisms at the microscale should be reflected at the macroscale. This quandary arises in both hierarchical and semiconcurrent multiscale methods. It is well known that failure in micromodels of composites and metals leads to fracture and shear bands at the macroscale. Similarly, when the micromodel is atomistic, failure of bonds leads to fracture and dislocations at the coarser scale. An effective multiscale methods must be able to model the inception of these phenomena as predicted by the subscale model.

It is often advanced that these difficulties can be circumvented by using rate-dependent material models at the macroscale. However, even for rate-dependent materials, when the underlying rate-independent model loses ellipticity, severe localization of deformation takes place. Accurate modeling of this localization in the macromodel requires extreme mesh refinement, which is computationally very expensive and sometimes impossible from a practical viewpoint.

The macroscale failure problem can be regularized by nonlocal and gradient methods; early forms of regularization are given in Bazant *et al.* [5], Lasry and Belytschko [6]. Kouznetsova *et al.* [7] and Vernerey *et al.* [8] have linked rate-independent failure models across scales with gradient methods. However, gradient and nonlocal methods also tend to exhibit significant localization when the underlying rate-independent constitutive model loses ellipticity. Furthermore, material instability is often associated with cracking and in the modeling of cracks at the macroscale, gradient methods can become quite ineffective. In fact such models treat cracks similar to phase field models, and several elements must span a crack for reasonable accuracy, particularly for cracks that are not coincident with mesh edges.

An alternative approach is that based on eigenstrains, which has recently been developed by Fish and Yuan [9] and Oskay and Fish [10]. The eigenstrain method has some distinctive advantages, such as computational efficiency, and it may be able to match some of the capabilities of the proposed method. However, it is significantly more complicated.

In Belytschko *et al.* [11], a multiscale method called multiscale aggregating discontinuities (MAD) was presented. The essential feature of the MAD method is that when material instabilities, such as cracks or shear bands, occur in the micromodel, an equivalent discontinuity is computed and injected into the macromodel. This is accomplished by removing the subdomain of the micromodel in which the material loses convexity from the domain used for computing the average strain and stress in the micromodel; these are the variables by which the micromodel communicates with the macromodel. Note that loss of convexity differs from loss of ellipticity in that it corresponds to a stronger condition associated with loss of positive definiteness of the material tangent matrix; this

DOI: 10.1002/nme

is discussed further in Section 7. The behavior of the subdomain that does not maintain convexity is reflected in the macromodel by a discontinuity. This is consistent with observed physical behavior: for example, fracture at the macroscale is often reflected by extensive arrays of cracks at the microscale.

The discontinuity at the macroscale is treated by the extended finite element method (XFEM) [12, 13], but any other method can also be used. The XFEM is advantageous since it accurately models cracks and other discontinuities with arbitrary alignments with respect to the mesh.

The topic of coarse-graining fracture is relatively unexplored. Aside from [11], one of the few studies is by Massart *et al.* [14], who have presented a method for linking failure of mortar to coarse scale discontinuities. However, they used a different method.

In this paper, improvements of [11] for coarse-graining failure are presented. The new features are:

1. better boundary conditions for unit cells with cracks,
2. development of equivalent non-constant cracks,
3. the use of the hourglass modes on the unit cell of the microstructure so that micromodel deformations with growing cracks are modeled more effectively.

It was shown in [11] that as a consequence of the redefined average stress and strain, the macromodel maintains ellipticity. This is important, since it insures that the solution of the macromodel will not suffer from ill-posedness and consequent spurious mesh-size dependence. We were unable to show this for the method described here. The addition of the hourglass modes unfortunately invalidates the proof of the strong ellipticity of the bulk material at the macroscale. We do show that the tangent stiffness matrix of the bulk material remains positive definite.

It should again be stressed that conventional coarse-graining methods, many of which are homogenization methods, such as those described in Zohdi and Wriggers [1] and Nemat-Nasser and Hori [15], are not applicable to failure analysis. All of these methods assume a periodic response and do not account for localization of deformation. Coarse graining in the presence of failure is distinctly different; hence, a whole new vista remains to be explored in extending multiscale methods to failure problems.

2. A TAXONOMY OF MULTISCALE METHODS

In order to delineate to which classes of multiscale approaches the proposed method is applicable, we will first describe a more detailed taxonomy of multiscale methods than is commonly given (parts of this taxonomy were given in Belytschko *et al.* [16]). Usually, multiscale methods are classified as:

1. hierarchical methods (also called sequential and information passing methods), where information is passed from the microscale to the macroscale,
2. concurrent methods, where the microscale model is strongly coupled with the macroscale model and run concurrently.

These two types of multiscale methods are illustrated in Figures 1(a) and (b), respectively, where we have shown the application of multiscale methods at ‘hot spots’, subdomains where failure has been determined likely to take place (perhaps by a previous simulation). However, there are several variants of multiscale techniques that fall between these extremes as shown in Table I.

DOI: 10.1002/nme

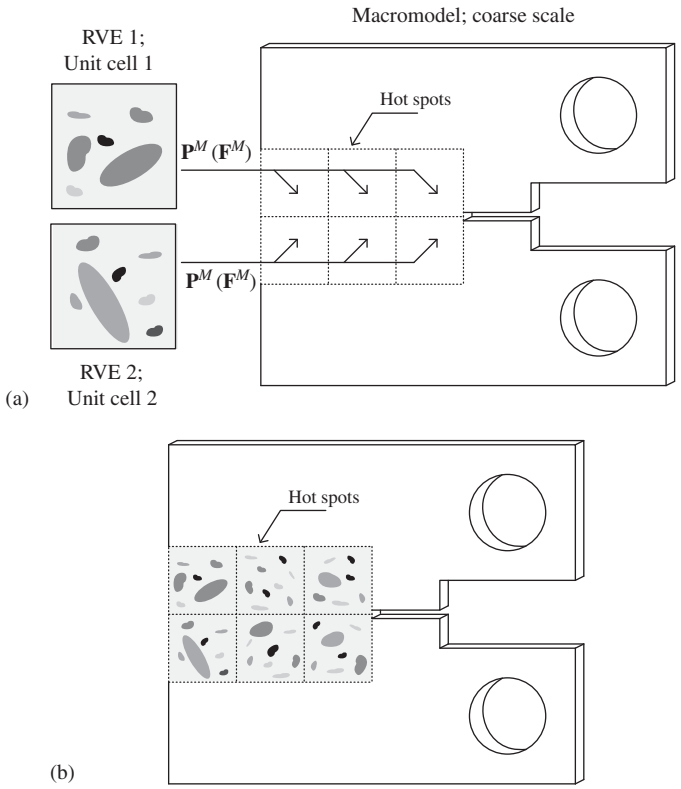

Figure 1. Schematic of models for: (a) hierarchical and (b) concurrent multiscale methods.

Table I. Taxonomy of multiscale methods.

Multiscale techniques	Information transfer	Interface conditions
Hierarchical	$\Omega^{\text{micro}} \rightarrow \Omega^{\text{Macro}}$	Weak
Hybrid hierarchical/ semiconcurrent	$\Omega^{\text{micro}} \rightarrow \Omega^{\text{Macro}}$ if $\mathbf{E}^{\text{M}} \in \varepsilon_F$ $\Omega^{\text{micro}} \leftrightarrow \Omega^{\text{Macro}}$ if $\mathbf{E}^{\text{M}} \notin \varepsilon_F$	Weak
Semiconcurrent	$\Omega^{\text{micro}} \leftrightarrow \Omega^{\text{Macro}}$	Weak
Concurrent	$\Omega^{\text{micro}} \Leftrightarrow \Omega^{\text{Macro}}$	Momentum balance and compatibility

$\rightarrow$, $\leftrightarrow$: weak coupling, $\Leftrightarrow$: strong coupling.
$\mathbf{E}^{\text{M}}$ = Green–Lagrangian strain; ε = domain on which repose to $\mathbf{E}^{\text{M}}$ is available.

As shown in Figure 1(a), in hierarchical methods, the response map $\mathbf{P}^{\text{M}}(\mathbf{F}^{\text{M}})$ is precomputed for a domain of inputs, where $\mathbf{P}^{\text{M}}$ is the coarse-grained nominal stress, and $\mathbf{F}^{\text{M}}$ is the coarse-grained deformation gradient. The outputs are then stored in some form, such as the parameters of a constitutive equation, a data base, or a neural network. When the coarse-scale model is run, this

DOI: 10.1002/nme

response map is interrogated to obtain the coarse-grained stresses. For example, in the hierarchical analysis of a two-scale continuum model, a microstructure model is used to obtain the stress response for the domain of strains anticipated in the coarse-scale simulation.

Concurrent methods are those in which the fine-scale model is embedded and strongly coupled with the coarse-scale model as show in Figure 1(b). By strong coupling, we mean that equilibrium (or momentum balance in the case of dynamics) and compatibility are enforced across the interface between the macromodel and the micromodel, and the micro and macromodels are solved simultaneously. For example, if some part of the macromodel requires a detailed subscale analysis to predict failure, the fine-scale model can be embedded in that subdomain of the coarse-scale model. The methods of Guidault *et al.* [17] and Ibrahimbegovic and Markovic [18] are in this class. Many atomistic/continuum multiscale methods are of this type. For example, in Abraham *et al.* [19] and Khare *et al.* [20], the atomistic and quantum domains are embedded in a continuum domain, and in Xiao and Belytschko [21] and Wagner and Liu [22], atomistic domains are embedded in continuum domains.

Concurrent methods can be viewed as domain decomposition methods: the domain is decomposed into fine-scale and coarse-scale models. The complete model is then solved with strong coupling between the subdomains. For more details, see Curtin and Miller [23] and Belytschko *et al.* [16].

Several methods fall in the spectrum between hierarchical and concurrent methods. One class, which we will call semiconcurrent methods, calculates the fine-scale model response for a specific input required by the coarse-scale model and passes the information to the coarser scale during the simulation of the coarse-scale model as shown in Figure 2. The fine-scale model is not closely coupled with the coarse-scale model, i.e. momentum balance and compatibility are not exactly enforced on the interface, although certain aspects of the two conditions are enforced. A classic example of this type of method is the FE^2 method [24, 25], where for each quadrature point in the coarse-scale finite element mesh, a fine-scale finite element mesh is used to compute the coarse-scale stress.

In semiconcurrent methods, the strain in the coarse-scale model at every step of the solution evolution is used to provide displacement boundary conditions for the fine-scale model. The fine-scale model is solved to obtain the fine-scale stresses, which are translated to the coarse-scale stresses by the Hill formulas and passed to the macromodel. This approach can be viewed as a means of computing the constitutive model *during the simulation*, *i.e.* '*on-the-fly*'. Another way to view this approach is that the kinematic and kinetic coupling are weak: the dimensionality (degrees-of-freedom) of the kinetic and kinematic variables that are passed between the macroscale and microscale is much lower than the dimensionality of the micromodel. An advantage of semiconcurrent methods over hierarchical methods is that it is not necessary to have a framework for storing the constitutive response.

In the hybrid-semiconcurrent multiscale approach, the fine-scale model is used to obtain the stress response (output) for a domain of strains (input) as in the hierarchical method. These are used in the coarse-scale simulation, but the fine-scale model is kept in readiness in case any strain in the coarse scale model is outside the precomputed strain domain. In that case, the fine-scale model is invoked in a semiconcurrent mode.

It can be argued that both the semiconcurrent methods are in essence hierarchical. However, the implementation is substantially different. In hierarchical methods, the fine-scale model is run first, and a complete description of its response is obtained. Semiconcurrent methods do not require this step because the response is generated on-the-fly during the simulation.

DOI: 10.1002/nme

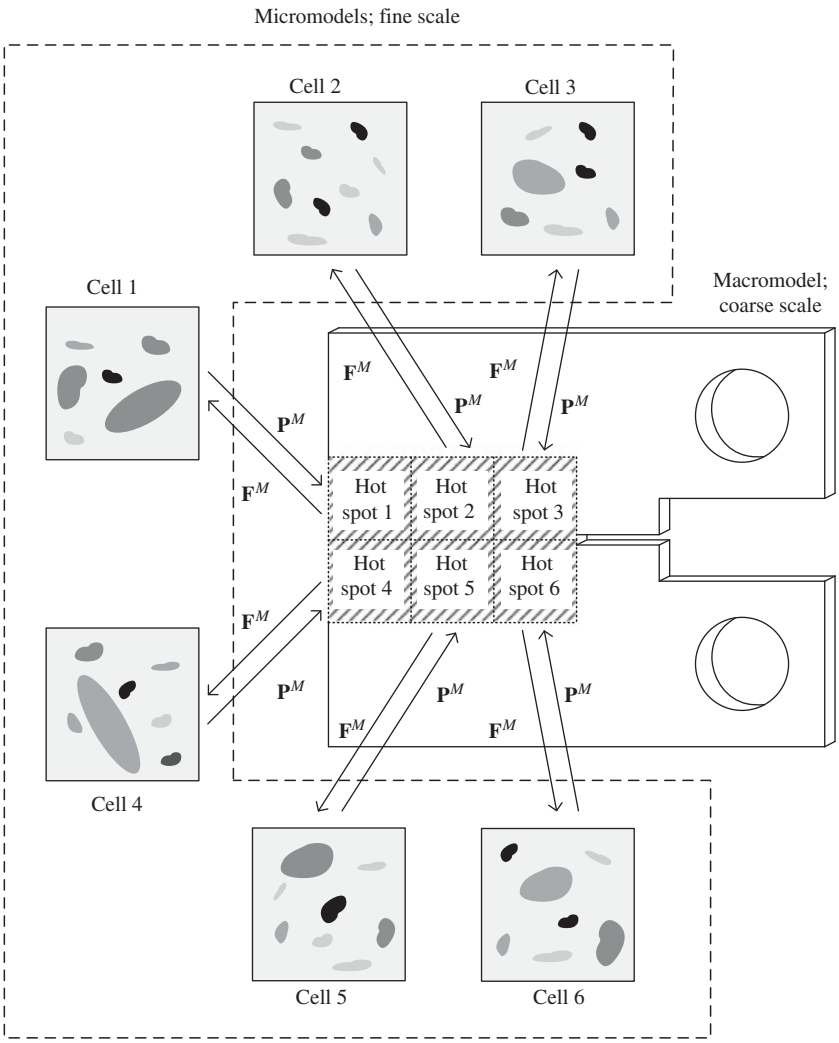

Figure 2. Schematic of a semiconcurrent multiscale method.

The proposed method is applicable to hierarchical, semiconcurrent and the hybrid multiscale methods. Indeed, the basic concept of injecting a discontinuity upon loss of ellipticity at the coarse scale is essential for linking any subscale model to a classical continuum theory, i.e. one without gradient, nonlocal, or other regularization, when the coupling is not concurrent.

3. OVERVIEW OF THE METHOD

The objectives of this paper were listed previously. Here we will consider the motivations for these objectives in more detail and provide an overview of the higher-order MAD method proposed here.

DOI: 10.1002/nme

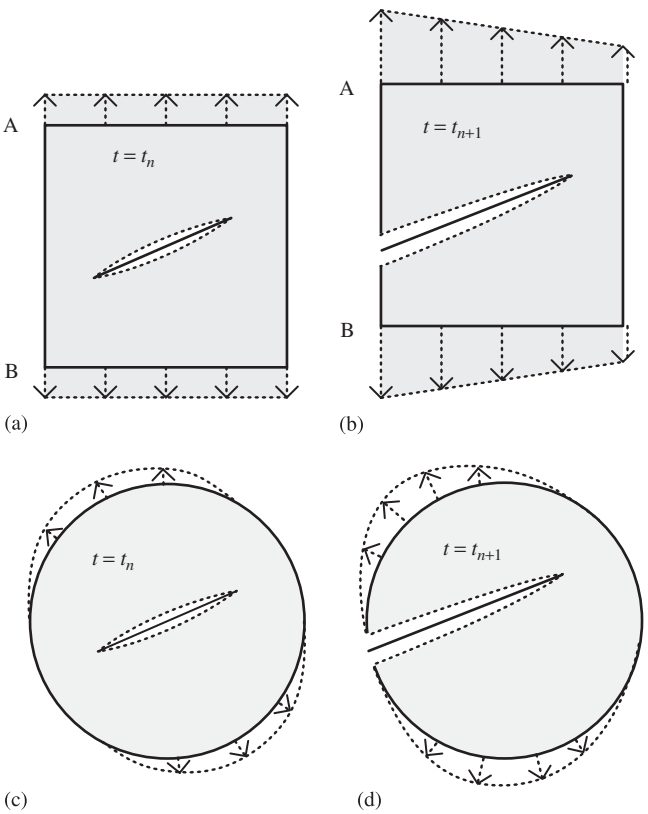

Figure 3. Crack growth with the crack penetrating edge AB for time $t_{n+1} > t_n$ for: (a) and (b) square unit cells, and (c) and (d) circular unit cells.

The first objective deals with difficulties arising in the situation depicted in Figure 3. Consider a crack that nucleates at the center of unit cell as shown in Figure 3(a), then grows to the left, and then penetrates the side AB as shown in Figure 3(b). The standard procedure for prescribing the displacements of the boundary of the unit cell is

$$\mathbf{u}^{\mathrm{m}}(\mathbf{X}^{\mathrm{m}}) = (\mathbf{F}^{\mathrm{M}}(\mathbf{X}^{\mathrm{M}}) - \mathbf{I}) \cdot \mathbf{X}^{\mathrm{m}} + \boldsymbol{\omega}(\mathbf{X}^{\mathrm{m}}), \quad \mathbf{X}^{\mathrm{m}} \in \Gamma_0^{\mathrm{m}} \quad \text{and} \quad \mathbf{X}^{\mathrm{M}} \in \Omega_0^{\mathrm{M}} \tag{1}$$

where $\mathbf{u}^{\mathrm{m}}$ is the microscale displacement, $\mathbf{F}^{\mathrm{M}}$ is the macroscale deformation gradient, $\mathbf{I}$ is the second-order unit tensor, $\boldsymbol{\omega}$ is the fluctuation in the micro-displacement field, and $\mathbf{X}$ is the material coordinate; superscripts m and M refer to the microscale and macroscale, respectively. The microscale displacement $\mathbf{u}^{\mathrm{m}}$ in Equation (1) does not account for the jump in displacement at the intersection of the crack with the edge; hence, it will be inconsistent with the microscale displacement field given in Equation (1). Therefore, methods that account for situations where cracks penetrate the surface of the unit cell need to be introduced.

We have shown two types of unit cells in Figure 3: square unit cells and circular unit cells. The latter were also used in Belytschko *et al.* [11]. Circular unit cells are of particular advantage in coarse graining of micromodels with crack growth because they avoid the difficulties arising from corners and provide a way to characterize in more detail cracks that do not span the unit cell.

DOI: 10.1002/nme

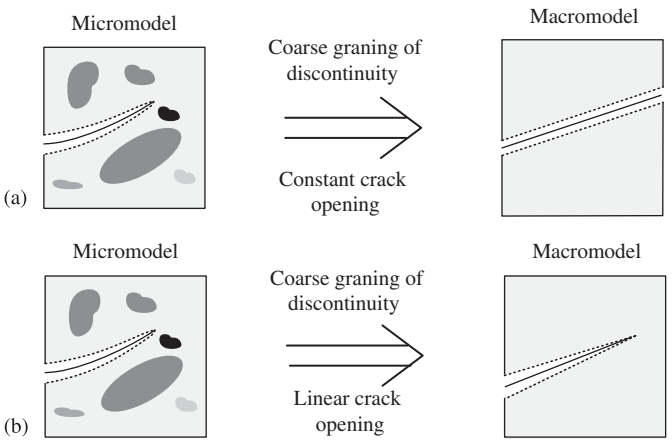

Figure 4. Schematic of coarse graining of a crack at the macroscale: (a) according to the original MAD method [11], and (b) the proposed MAD method.

The second difficulty is illustrated in Figure 4. In Belytschko *et al.* [11], cracks in the micromodel were coarse-grained by a single discontinuity with constant crack opening and smoothing schemes were used to construct a smoothly opening crack at the coarse scale. Here, we propose a method where the crack opening that is passed to the coarse-grained model can vary linearly in the macroelement. Moreover, we have added techniques to model nucleating cracks. These techniques provide a substantially better representation of the discontinuities at the macroscale.

The motivation for the third objective is illustrated in Figure 5. When a crack opens and grows, the deformation of a unit cell is approximately that shown in Figure 5. This mode of deformation cannot be effectively represented with Equation (1) for the deformation associated with an opening crack is a bilinear displacement field, often called an hourglass mode or bilinear mode in the finite element literature [26, 27]. The inadequacy of constant deformation modes should be clear from the schematic of the constant deformation gradient modes shown in Figure 6. Although the constant mode F_{yx} has similarities with the hourglass mode shown in Figure 5, it is characterized by shear, whereas the crack-opening mode shown in Figure 5 should be a tensile mode with linearly varying F_{yy}.

The bilinear displacement mode shown in Figure 5 has a linearly varying extensional deformation gradient, F_{yy} and this is what has been added in this work. To obtain this mode, the boundary displacements must vary like XY, which is the hourglass mode. In many situations, particularly those involving a single crack or a dominant crack near percolation, effective modeling of crack growth requires that the hourglass mode be included in the deformation of the unit cell. Incidentally, we have only shown the y-hourglass mode in Figure 5; a similar x-hourglass mode, i.e. for the x-component of the displacement field, is also considered.

As in Belytschko *et al.* [11], we employ two key concepts for coarse-graining multiscale failure phenomena:

1. all averaging operations are performed over a 'perforated' unit cell that excludes all subdomains that lose convexity (to be defined later); these can be loosely considered subdomains where material stability is lost (areas of material instability, which of course, include cracks),

DOI: 10.1002/nme

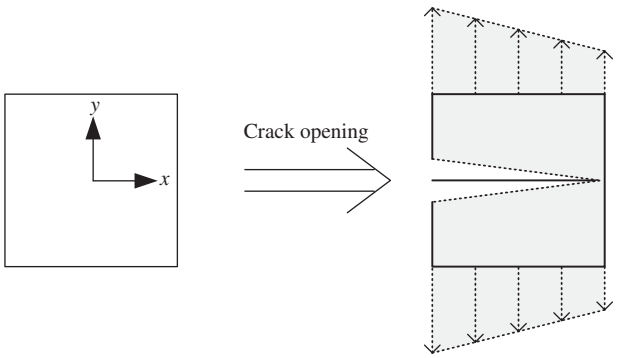

Figure 5. Schematic of crack opening; showing the importance of the hourglass mode.

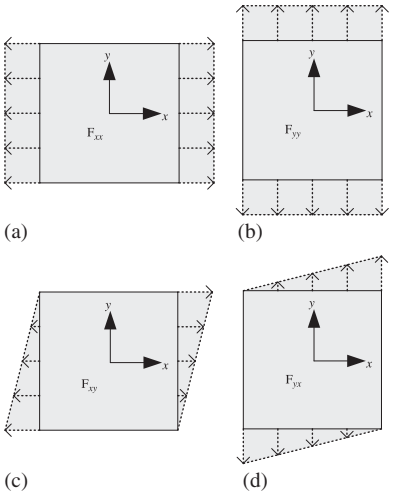

Figure 6. Schematic of constant deformation gradient modes.

2. a formula is developed whereby the discontinuous and localized deformations in a unit cell are replaced by a single equivalent discontinuity.

It is assumed that the size scale of the microscale models, l^c, i.e. the unit cells, is of order h, where h is the length of a typical finite element in the macromodel. In contrast to representative volume elements in homogenization theories, the method is not independent of l^c.

4. COARSE-GRAINING METHOD

The developments in this section will be described for two-dimensional problems, although they can be extended to three dimensions. In many cases, we give equations applicable to both two or three dimensions, but we limit the detailed formulation to two dimensions.

As before, the superscripts M and m refer to the macroscale and microscale, respectively. The method can easily be translated for an analysis at several scales by letting $M = K$, $m = K + 1$ for

DOI: 10.1002/nme

whatever pair of scales is being considered, which is the notation used in [11]. The reference domain of the macromodel is denoted by Ω_0^{M} and its boundary by Γ_0^{M}.

The domain of the perforated unit cell is denoted by $\tilde{\Omega}_0^{\mathrm{m}}$, hence,

$$\tilde{\Omega}_0^{\mathrm{m}} = \Omega_0^{\mathrm{m}} \setminus \Omega_0^{\mathrm{uns}} \tag{2}$$

where Ω_0^{uns} is the subdomain of the unit cell where the material is not convex; this could be an area of localization of strain. Any crack is excluded from Ω_0, even though it is a set of measure zero, since the material must lose convexity as the stress goes to zero on the crack plane. The implications of this are rather delicate for cracks, and are discussed in a forthcoming paper. We just note that as a consequence, any cohesive stress is not included in the averaging operation.

All averaging operations are performed over the perforated unit cell; hence, denoting the averaging operation by $\langle\cdot\rangle$, we have for any function $f(\mathbf{X}^{\mathrm{m}})$:

$$\langle f(\mathbf{X}^{\mathrm{m}})\rangle = \frac{1}{|\tilde{\Omega}_0^{\mathrm{m}}|}\int_{\tilde{\Omega}_0^{\mathrm{m}}} f(\mathbf{X}^{\mathrm{m}})\,\mathrm{d}\Omega_0 \tag{3}$$

where $|\cdot|$ denotes the measure of the domain, such as the area in two dimensions or the volume in three dimensions. The macroscale deformation gradient $\mathbf{F}^{\mathrm{M}}$ and the macroscale first Piola–Kirchoff stress $\mathbf{P}^{\mathrm{M}}$ are defined as the averages of the microscale deformation gradient $\mathbf{F}^{\mathrm{m}}$ and the microscale first Piola–Kirchhoff stress $\mathbf{P}^{\mathrm{m}}$ over the perforated unit cell, respectively, hence

$$\langle \mathbf{F}^{\mathrm{m}}\rangle = \frac{1}{|\tilde{\Omega}_0^{\mathrm{m}}|}\int_{\tilde{\Omega}_0^{\mathrm{m}}} \mathbf{F}^{\mathrm{m}}\,\mathrm{d}\Omega_0 \tag{4}$$

$$\langle \mathbf{P}^{\mathrm{m}}\rangle = \frac{1}{|\tilde{\Omega}_0^{\mathrm{m}}|}\int_{\tilde{\Omega}_0^{\mathrm{m}}} \mathbf{P}^{\mathrm{m}}\,\mathrm{d}\Omega_0 \tag{5}$$

To treat the hourglass modes, two generalized hourglass strains $\mathbf{q}=[q_1, q_2]$ and two corresponding generalized stresses $\mathbf{Q}=[Q_1, Q_2]$ are added to the kinematic and kinetic descriptions at the macroscale. These extra generalized stresses and strains are assumed to be energetically consistent with the work in the perforated unit cell so that

$$\mathbf{P}^{\mathrm{M}} : \delta\mathbf{F}^{\mathrm{M}} + \mathbf{Q}\cdot\delta\mathbf{q} = \frac{1}{|\tilde{\Omega}_0|}\int_{\tilde{\Omega}_0^{\mathrm{m}}} \mathbf{P}^{\mathrm{m}} : \delta\mathbf{F}^{\mathrm{m}}\,\mathrm{d}\Omega_0 \tag{6}$$

The introduction of additional modes is in the same spirit as in Kouznetsova *et al.* [7], but only the first higher-order generalized stresses and strains are considered.

The macrocrack is an approximation to either a single crack or a group of cracks at the microscale. The cracks at the microscale are described by

$$f_\beta^{\mathrm{m}}(\mathbf{X}^{\mathrm{m}}) = 0 \quad \text{and} \quad g_\beta^{\mathrm{m}}(\mathbf{X}^{\mathrm{m}}) > 0 \tag{7}$$

where $f_\beta^{\mathrm{m}}(\mathbf{X}^{\mathrm{m}})$ describes the surface of the crack β and $g_\beta^{\mathrm{m}}(\mathbf{X}^{\mathrm{m}})$ describes its extent. The crack path at the microscale may be jagged, but it is assumed that the crack path penetrates the walls of the unit cells at no more than two points. If the front of crack β is within the unit cell, it is given by

$$f_\beta^{\mathrm{m}}(\mathbf{X}^{\mathrm{m}}) = g_\beta^{\mathrm{m}}(\mathbf{X}^{\mathrm{m}}) = 0 \tag{8}$$

A typical crack at the microscale and its macroscale equivalent is shown in Figure 7.

DOI: 10.1002/nme

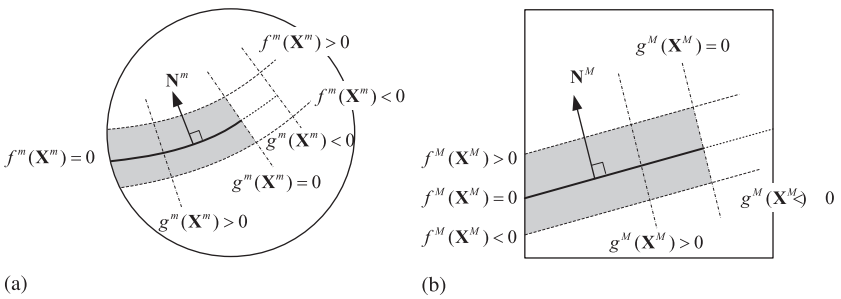

Figure 7. Relation of cracks at: (a) the microscale and (b) the macroscale.

The geometry of the equivalent macrocrack in a neighborhood corresponding to the unit cell is described by an affine level set function

$$f^{\mathrm{M}}(\mathbf{X}^{\mathrm{M}}) = \alpha_0 + \alpha_\beta X^{\mathrm{M}}_\beta = 0, \quad \beta = 1 \text{ to } 2 \tag{9}$$

where α_0 and α_β are parameters obtained from the coarse-graining. In addition, to describe the ends of the crack, we introduce a second level set function $g^{\mathrm{M}}(\mathbf{X}^{\mathrm{M}})$ and define it so that on the crack $g^{\mathrm{M}}(\mathbf{X}^{\mathrm{M}}) \geqslant 0$.

The motion $\boldsymbol{\phi}^{\mathrm{m}}(\mathbf{X}^{\mathrm{m}})$ on the outside boundary of the unit cell given by

$$\boldsymbol{\phi}^{\mathrm{m}}(\mathbf{X}^{\mathrm{m}}) = \mathscr{F}^{\mathrm{M}} \cdot \mathbf{X}^{\mathrm{m}} + \mathbf{q} XY + \boldsymbol{\omega}(\mathbf{X}^{\mathrm{m}}), \quad \mathbf{X}^{\mathrm{m}} \in \Gamma_0^{\mathrm{m}} \tag{10}$$

where in two dimensions $\mathbf{q}^{\mathrm{T}} = [q_x, q_y]$. The second term in Equation (10) accounts for the hourglass modes; $\mathbf{q}$ is obtained from the macroscale deformation as described later. The second term is one of the key differences from the previously presented MAD method [11]. Henceforth we drop the fluctuations $\boldsymbol{\omega}(\mathbf{X})$ since the MAD method is not used with periodic boundary conditions.

Equation (10) is not consistent with a crack penetrating the surface, i.e. in the neighborhood of $f^{\mathrm{m}}(\mathbf{X}^{\mathrm{m}}) = 0$, unless the crack displacement on the surface is considered as part of the fluctuations. Therefore, if the motion of the boundary is completely described by (10), the motion will not be consistent with a cracking unit cell. In fact, the motion prescribed by Equation (10) will tend to arrest the crack as it approaches the boundary.

To avoid this effect, we switch from a prescribed displacement boundary condition to a prescribed traction boundary condition in a neighborhood of the crack, i.e. intersection of the shaded region with the periphery of the circle in Figure 7(a). If we denote this portion of the boundary by $\Gamma_0^{\mathrm{m}P}$ and the prescribed displacement portion by $\Gamma_0^{\mathrm{m}F}$, then the boundary condition becomes

$$\bar{\boldsymbol{\phi}}^{\mathrm{m}}(\mathbf{X}^{\mathrm{m}}) = \mathscr{F}^{\mathrm{M}} \cdot \mathbf{X}^{\mathrm{m}} + \mathbf{q} XY, \quad \mathbf{X}^{\mathrm{m}} \in \Gamma_0^{\mathrm{m}F} \tag{11}$$

$$\bar{\mathbf{t}}^{\mathrm{m}}(\mathbf{X}^{\mathrm{m}}) = \langle \mathbf{P}^{\mathrm{m}} \rangle \cdot \mathbf{N}^{\mathrm{m}}(\mathbf{X}^{\mathrm{m}}), \quad \mathbf{X}^{\mathrm{m}} \in \Gamma_0^{\mathrm{m}P} \tag{12}$$

where $\bar{\boldsymbol{\phi}}^{\mathrm{m}}$ and $\bar{\mathbf{t}}^{\mathrm{m}}$ are the prescribed displacement and traction along $\Gamma_0^{\mathrm{m}F}$ and $\Gamma_0^{\mathrm{m}P}$, respectively. Note that the above requires an iterative procedure, since the stress $\langle \mathbf{P}^{\mathrm{m}} \rangle$ is not known until the solution for the unit cell has been obtained. This procedure consists of obtaining $\langle \mathbf{P}^{\mathrm{m}} \rangle^{\mathrm{new}}$, and then solving the unit cell. The procedure converged in our examples, but requires further study.

DOI: 10.1002/nme

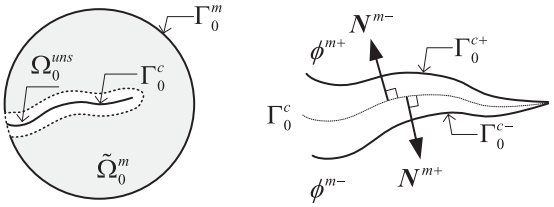

Figure 8. Nomenclature for crack surfaces and normals.

We next describe how the magnitude of the discontinuity and the normal to the discontinuity at the macroscale are extracted from the unit cell deformation. We will use the following equation for this purpose:

$$|\tilde{\boldsymbol{\Omega}}_0^{\mathrm{m}}|(\langle \mathbf{F}^{\mathrm{m}} \rangle - \mathscr{F}^{\mathrm{M}}) + \int_{\Gamma_0^c} [\![\boldsymbol{\phi}^{\mathrm{m}} \otimes \mathbf{N}^{\mathrm{m}}]\!] \, \mathrm{d}\Gamma_0 = 0 \tag{13}$$

This equation holds only if a crack does not penetrate through the walls of the unit cell, but we will use it for the mixed conditions described above. To obtain this equation, we note that

$$\langle \mathbf{F}^{\mathrm{m}} \rangle = \frac{1}{|\tilde{\boldsymbol{\Omega}}_0^{\mathrm{m}}|} \int_{\tilde{\Omega}_0^{\mathrm{m}}} \mathbf{F}^{\mathrm{m}} \, \mathrm{d}\Omega_0 = \frac{1}{|\tilde{\boldsymbol{\Omega}}_0^{\mathrm{m}}|} \int_{\tilde{\Omega}_0^{\mathrm{m}}} \nabla_0 \otimes \boldsymbol{\phi}^{\mathrm{m}} \, \mathrm{d}\Omega_0 \tag{14}$$

By the divergence theorem

$$\int_{\tilde{\Omega}_0^{\mathrm{m}}} \nabla_0 \otimes \boldsymbol{\phi}^{\mathrm{m}} \, \mathrm{d}\Omega_0 = \int_{\Gamma_0^m \setminus \Gamma_0^c} \boldsymbol{\phi}^{\mathrm{m}} \otimes \mathbf{N}^{\mathrm{m}} \, \mathrm{d}\Gamma_0 - \int_{\Gamma_0^c} [\![\boldsymbol{\phi}^{\mathrm{m}} \otimes \mathbf{N}^{\mathrm{m}}]\!] \, \mathrm{d}\Gamma_0 \tag{15}$$

where

$$[\![\boldsymbol{\phi}^{\mathrm{m}} \otimes \mathbf{N}^{\mathrm{m}}]\!] = \boldsymbol{\phi}^{\mathrm{m}+} \mathbf{N}^{\mathrm{m}-} + \boldsymbol{\phi}^{\mathrm{m}-} \mathbf{N}^{\mathrm{m}+} \tag{16}$$

and

$$\boldsymbol{\phi}^{\mathrm{m}+} = \phi^{\mathrm{m}}(\mathbf{X}_{\Gamma_0^c}^{\mathrm{m}} + \varepsilon \mathbf{N}^{\mathrm{m}-}), \quad \boldsymbol{\phi}^{\mathrm{m}-} = \phi(\mathbf{X}_{\Gamma_0^c}^{\mathrm{m}} + \varepsilon \mathbf{N}^{\mathrm{m}+}), \quad \varepsilon \to 0 \tag{17}$$

where $\mathbf{N}^{\mathrm{m}+}$ and $\mathbf{N}^{\mathrm{m}-}$ are the normals to the top and the bottom surfaces of the microcrack; see Figure 8.

Substituting Equation (15) into (14) and using (10) give

$$|\tilde{\boldsymbol{\Omega}}_0^{\mathrm{m}}| \langle \mathbf{F}^{\mathrm{m}} \rangle = \int_{\Gamma_0^m \setminus \Gamma_0^c} \mathscr{F}^{\mathrm{M}} \cdot \mathbf{X}^{\mathrm{m}} \otimes \mathbf{N}^{\mathrm{m}} \, \mathrm{d}\Gamma_0 + \underbrace{\int_{\Gamma_0^m \setminus \Gamma_0^c} \mathbf{q} XY \otimes \mathbf{N}^{\mathrm{m}} \, \mathrm{d}\Gamma_0}_{=0} - \int_{\Gamma_0^c} [\![\boldsymbol{\phi}^{\mathrm{m}} \otimes \mathbf{N}^{\mathrm{m}}]\!] \, \mathrm{d}\Gamma_0 \tag{18}$$

where we have indicated in the above that since the origin of the coordinate system of the unit cell is taken to the center, the second term of the right-hand side vanishes. The first term can be

DOI: 10.1002/nme

simplified by the following steps:

$$\int_{\Gamma_0^m \setminus \Gamma_0^c} \mathscr{F}^{\mathrm{M}} \cdot \mathbf{X}^{\mathrm{m}} \otimes \mathbf{N}^{\mathrm{m}} \, \mathrm{d}\Gamma_0 = \mathscr{F}^{\mathrm{M}} \cdot \int_{\Gamma_0^m \setminus \Gamma_0^c} \mathbf{X}^{\mathrm{m}} \otimes \mathbf{N}^{\mathrm{m}} \, \mathrm{d}\Gamma_0 \tag{19}$$

$$= \mathscr{F}^{\mathrm{M}} \int_{\tilde{\Omega}_0^{\mathrm{m}}} \nabla_0 \otimes \mathbf{X}^{\mathrm{m}} \, \mathrm{d}\Omega_0 \tag{20}$$

$$= |\tilde{\mathbf{\Omega}}_0^{\mathrm{m}}| \mathscr{F}^{\mathrm{M}} \tag{21}$$

Hence,

$$\int_{\Gamma_0^c} [\![\boldsymbol{\phi}^{\mathrm{m}} \otimes \mathbf{N}^{\mathrm{m}}]\!] \, \mathrm{d}\Gamma_0 = |\tilde{\mathbf{\Omega}}_0^{\mathrm{m}}| (\langle \mathscr{F}^{\mathrm{m}} \rangle - \mathbf{F}^{\mathrm{M}}) \equiv |\tilde{\mathbf{\Omega}}_0^{\mathrm{m}}| \mathbf{F}_E^{\mathrm{M}} \tag{22}$$

which concludes the derivation of Equation (13). This relation is identical to the relation for the standard unit cell; it is independent of $\mathbf{q}$. The above is a generalization of Hill's averaging theorem which is also given in Loehnert [28] and Belytschko *et al.* [11].

In coarse graining the crack, we wish to find a $\mathbf{U}^{\mathrm{M}}(\xi^{\mathrm{M}}) = [\![\boldsymbol{\phi}^{\mathrm{M}}(\xi^{\mathrm{M}})]\!]$ such that

$$\int_{\Gamma_0^c} \mathbf{U}^{\mathrm{M}} \otimes \mathbf{N}^{\mathrm{M}} \, \mathrm{d}\Gamma_0 = |\tilde{\mathbf{\Omega}}_0^{\mathrm{m}}| \mathbf{F}_E^{\mathrm{M}} \tag{23}$$

where

$$\mathbf{F}_E^{\mathrm{M}} = \mathscr{F}^{\mathrm{M}} - \langle \mathbf{F}^{\mathrm{m}} \rangle \tag{24}$$

Since the left-hand side of Equation (23) is of rank 1, whereas the right-hand side is of rank 3, in most cases, a vector $\mathbf{U}^{\mathrm{M}}$ that satisfies Equation (23) exactly cannot be found. Therefore, we obtain an estimate of $\mathbf{U}^{\mathrm{M}}$ and $\mathbf{N}^{\mathrm{M}}$ by minimizing

$$J^D = \left\| \int_{\Gamma_0^c} \mathbf{U}^{\mathrm{M}} \otimes \mathbf{N}^{\mathrm{M}} \, \mathrm{d}\Gamma_0 - |\tilde{\mathbf{\Omega}}_0^{\mathrm{m}}| \mathbf{F}_E^{\mathrm{M}} \right\|^2 \tag{25}$$

The integrand in the above depends on the topology of the crack at the macroscale. In all cases, we assume that the crack is planar within a macroelement; hence, $\mathbf{N}^{\mathrm{M}}$ is constant.

Some of the topologies considered are:

(1) if the crack has penetrated the left edge L, but not the right edge, then we assume a linear variation of the crack opening at the macroscale

$$\mathbf{U}^{\mathrm{M}}(\xi^{\mathrm{M}}) = \frac{\mathbf{U}_{\mathrm{L}}^{\mathrm{M}}}{2}(1 - \xi^{\mathrm{M}}) \tag{26}$$

where ξ^{M} is defined in Figure 9. A linear variation in the magnitude of the discontinuity is assumed because that is all the information that can be incorporated at the macroscale model. The quadratic form J^D is then given by substituting Equation (26) into Equation (25). Similar formulas can easily be developed for cracks that penetrate the right edge, the bottom or the top.

DOI: 10.1002/nme

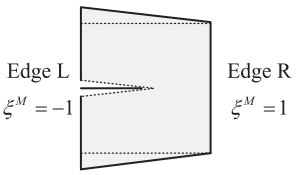

Figure 9. Definition of ξ^{M} at the macros element.

(2) If the crack penetrates both sides then

$$\mathbf{U}^{\mathrm{M}}(\xi^{\mathrm{M}}) = \tfrac{1}{2}(\mathbf{U}_{\mathrm{L}}^{\mathrm{M}}(1-\xi^{\mathrm{M}}) + \mathbf{U}_{\mathrm{R}}^{\mathrm{M}}(1+\xi^{\mathrm{M}})) \tag{27}$$

In that case, we use Equation (25) to obtain $\mathbf{U}^{\mathrm{M}} = \frac{1}{2}(\mathbf{U}_{\mathrm{L}}^{\mathrm{M}} + \mathbf{U}_{\mathrm{R}}^{\mathrm{M}})$ and obtain $\mathbf{U}_{\mathrm{L}}^{\mathrm{M}}$ and $\mathbf{U}_{\mathrm{R}}^{\mathrm{M}}$ as described in Section 5.

5. MICRO–MACRO LINKAGE

Both the microscale and macrocrack models are solved by the XFEM [12, 13, 29] approach, but the methodology applies to other methods for modeling cracks. An overview of the linkage is shown in Figure 10. As shown, the micromodel passes the stresses and the magnitude and direction of the discontinuity to the corresponding macroelement, $\mathbf{U}^{\mathrm{M}}$ and $\mathbf{N}^{\mathrm{M}}$, respectively. The discontinuity is directly injected into the macromodel as long as the micromodel is not completely cut into two, i.e. prior to percolation. The stress is passed to the quadrature point in the macroelement. The equations of equilibrium (or the momentum equation for dynamic processes) are then solved. In the solution process, the motion of the nodes adjusts for the injected discontinuity.

Once percolation has occurred in the micromodel, only the direction of the crack is passed to the macromodel. The magnitude of the discontinuity then becomes an unknown.

In cracked macroscale elements, the displacement field is given by

$$\mathbf{u}^h(\mathbf{X}^{\mathrm{M}}, t) = \sum_I \Psi_I(\mathbf{X}^{\mathrm{M}})\mathbf{u}_I(t) + \sum_J \Psi_J(\mathbf{X}^{\mathrm{M}}) H(f^{\mathrm{M}}(\mathbf{X}^{\mathrm{M}}) - f^{\mathrm{M}}(\mathbf{X}_J^{\mathrm{M}}))\mathbf{a}_J(t) \tag{28}$$

where $\Psi_I(\mathbf{X})$ are the element shape functions and $H(\cdot)$ is the Heaviside function. The level set function $f^{\mathrm{M}}(\mathbf{X}^{\mathrm{M}})$ must be chosen so that

$$\nabla_0 f^{\mathrm{M}}(\mathbf{X}^{\mathrm{M}}) = \mathbf{N}^{\mathrm{M}} \tag{29}$$

The condition in Equation (29) does not suffice to determine the level set function $f^{\mathrm{M}}(\mathbf{X}^{\mathrm{M}})$. The procedure for any element e is as follows:

(1) if a crack exists in an element adjacent to element e, the crack path, i.e. the level set function, is set so it is continuous between the two elements,
(2) if a crack nucleates in element e, it is centered in the element.

DOI: 10.1002/nme

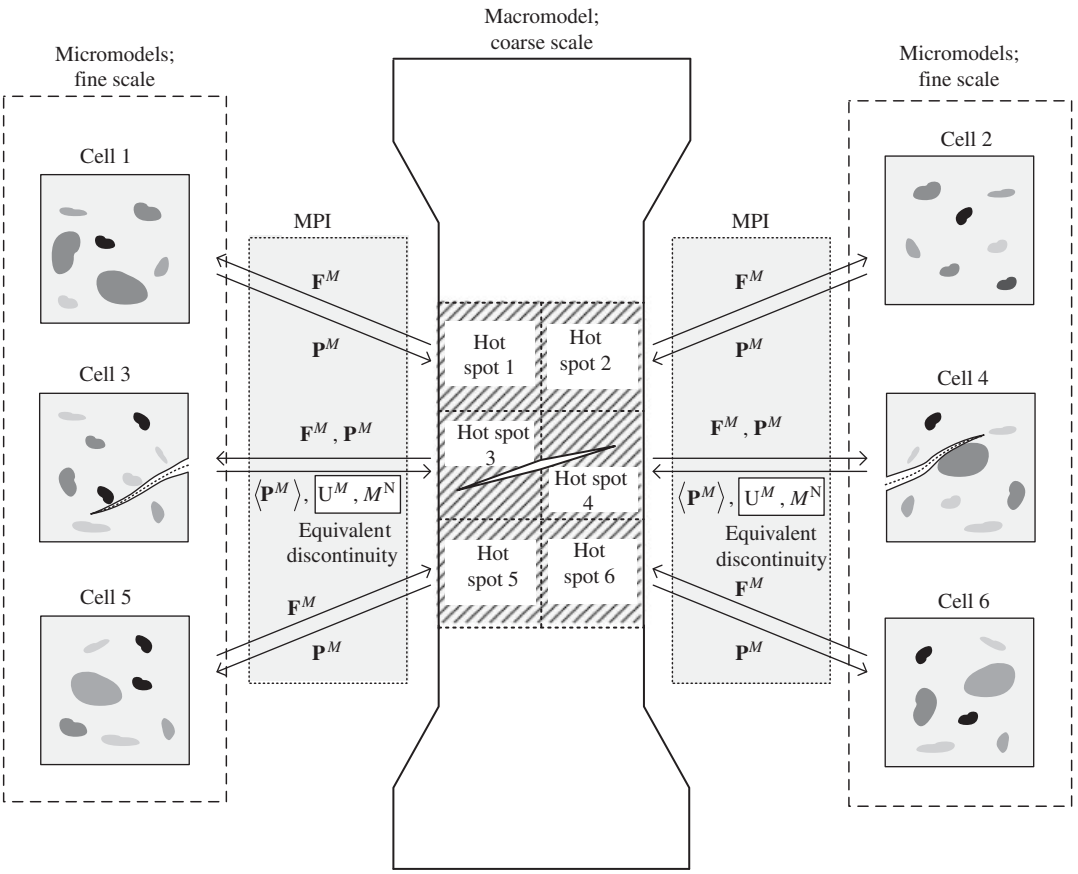

Figure 10. Schematic of macro–micro linkages of the MAD method.

The amplitude of crack opening, which is specified by $\mathbf{a}_J(t)$ in Equation (28), also requires matching between adjacent elements. The matching constraints for continuity of crack opening at interfaces between elements are written as a linear equation

$$\mathbf{Da} = \mathbf{b} \tag{30}$$

where $\mathbf{D}$ depends on the position of the crack and $\mathbf{b}$ is a linear function of $\mathbf{U}_{\mathrm{L}}$ and $\mathbf{U}_{\mathrm{R}}$ in the cracked elements. Note that the crack opening depends only on $\mathbf{a}$, and the above conditions are linear in $\mathbf{a}$.

The equations of motion then incorporate the above as constraints by Lagrange multipliers. The modified equation of motion is

$$\mathbf{M}\ddot{\mathbf{d}} = \mathbf{f} + \mathbf{D}^{\mathrm{T}}\boldsymbol{\lambda} = \mathbf{f}^{\mathrm{ext}} - \mathbf{f}^{\mathrm{int}} + \mathbf{D}^{\mathrm{T}}\boldsymbol{\lambda} \tag{31}$$

where $\mathbf{M}$ is the mass matrix, $\mathbf{d}$ is the matrix of degrees of freedom, $\mathbf{f}^{\mathrm{int}}$ is the nodal internal forces, and $\mathbf{f}^{\mathrm{ext}}$ is the nodal external forces, see Belytschko *et al.* [3]. The matrices $\mathbf{d}$ and $\mathbf{f}$ consist of the

DOI: 10.1002/nme

parts associated with the enriched parts emanating from XFEM, i.e.

$$\mathbf{d}_I^{\mathrm{T}} = \begin{Bmatrix} \mathbf{u}_I \\ \mathbf{a}_I \end{Bmatrix}, \quad \mathbf{f}_I^{\mathrm{T}} = \begin{Bmatrix} \mathbf{f}_I \\ \mathbf{A}_I \end{Bmatrix} \tag{32}$$

$$\mathbf{d}^{\mathrm{T}} = \{\mathbf{d}_I\}_{I=1}^{n_N}, \quad \mathbf{f}^{\mathrm{T}} = \{\mathbf{f}_I\}_{I=1}^{n_N} \tag{33}$$

where n_N is the number of nodes.

Crack nucleation can be treated by a new method similar to an s-method [30, 31], and the cracking particle method by Rabczuk and Belytschko [32]. The XFEM methods for crack nucleation were previously developed by Bellec and Dolbow [33] for elastic fracture mechanics. They use blending methods to combine two sets of the branch functions given in [33]. In this work, we model nucleating cracks by bubble functions.

The bubble function is developed as follows. Suppose that a nucleated crack with normal $\mathbf{N}^{\mathrm{M}}$ and length l^c appears in element e. We then let the displacement field in element e be

$$\mathbf{u}^h(\mathbf{X}^{\mathrm{M}}, t) = \sum_I \Psi_I(\mathbf{X}^{\mathrm{M}})\mathbf{u}_I(t) + \sum \Psi_J(\mathbf{X})\Phi(\xi^{\mathrm{M}})H(\mathbf{N}^{\mathrm{M}} \cdot (\mathbf{X}^{\mathrm{M}} - \bar{\mathbf{X}}_e^{\mathrm{M}}))\mathbf{a}_J(t) \tag{34}$$

where $\bar{\mathbf{X}}_e^{\mathrm{M}}$ is the center of the element e, $\Phi(\xi)$ is a cubic spline function given by

$$\Phi(\xi) = \begin{cases} 4\left(\dfrac{\xi}{l_c} - 1\right)\left(\dfrac{\xi}{l_c}\right)^2 + \dfrac{2}{3}, & 0 < \xi < 0.5 l_c \\ \dfrac{4}{3}\left(1 - \dfrac{\xi}{l_c}\right)^3, & 0.5 l_c \leqslant \xi \leqslant l_c \\ 0 & \text{otherwise} \end{cases} \tag{35}$$

6. CRACK OPENING IN UNIT CELLS WITH THE HOURGLASS MODE

As we described in the previous section, the motion of unit cells during failure processes cannot be solely driven by the constant deformation gradients that emanate from coarse-scale models, because the unit cell when crack opening takes place deforms primarily in a bilinear mode, also called the hourglass modes. A constant deformation gradient on the boundaries cannot represent this high-order motion.

Here, we will briefly describe the scheme for linking the bilinear mode from the coarse-scale model that is discretized with 4-node quadrilateral elements with the micromodel. The scheme for extracting the bilinear modes are based on Flanagan and Belytschko [26] and Belytschko and Bachrach [27]. In [26, 27], the extracted hourglass modes are used to control hourglass modes due to one-point quadrature 4-node quadrilateral elements. Here we use them to link the higher-order modes of the coarse-scale model with the fine-scale model.

Following Flanagan and Belytschko [26], the bilinear mode is computed by

$$q_i = \sum_I u_{iI}\gamma_I \tag{36}$$

DOI: 10.1002/nme

where $\mathbf{u}_I$ is the nodal displacement of the finite element and $\boldsymbol{\gamma}_I$ is the hourglass mode projection operator defined by

$$\boldsymbol{\gamma}_I = \frac{1}{4}\left\{\mathbf{h}_I - \left(\sum_J \mathbf{h}_J \mathbf{X}_J\right)\mathbf{b}_I^X - \left(\sum_J \mathbf{h}_J \mathbf{Y}_J\right)\mathbf{b}_I^Y\right\} \tag{37}$$

where $\mathbf{X}_I$ and $\mathbf{Y}_J$ is the X and Y components of the current nodal coordinates of the finite element, respectively, and $\mathbf{h}$ and $\mathbf{b}$ are defined as

$$\mathbf{h}^{\mathrm{T}} = [1 \;\; -1 \;\; 1 \;\; -1] \tag{38}$$

$$\begin{bmatrix} \mathbf{b}_I^X \\ \mathbf{b}_I^Y \end{bmatrix} = \begin{bmatrix} \partial \Psi_I(\mathbf{0})/\partial X \\ \partial \Psi_I(\mathbf{0})/\partial Y \end{bmatrix} \tag{39}$$

Note that strictly speaking $\mathbf{q}$ is the strength of the bilinear mode in the referential coordinates, but we ignore this difference.

The macrostresses are linked to the unit cell as follows. We use the generalized Hill–Mandel energetic relations in Equation (6). Substituting the displacement field in Equation (10) into Equation (6), we obtain the following expressions for the macrostresses:

$$\mathbf{P}^{\mathrm{M}} = \frac{1}{|\tilde{\Omega}_0^{\mathrm{m}}|}\int_{\Gamma_0^m} \mathbf{P}^{\mathrm{m}} \cdot \mathbf{N}^{\mathrm{m}} \otimes \mathbf{X}\, \mathrm{d}\Gamma_0 \tag{40}$$

$$\mathbf{Q} = \frac{1}{|\tilde{\Omega}_0^{\mathrm{m}}|}\int_{\Gamma_0^m} \mathbf{P}^{\mathrm{m}} XY \cdot \mathbf{N}^{\mathrm{m}}\, \mathrm{d}\Gamma_0 \tag{41}$$

The expressions for the nodal forces of a 4-node quadrilateral element [26] are

$$f_{iI}^{\mathrm{int}} = \int_{\Omega_0^{\mathrm{M}}} \frac{\partial \Psi_I}{\partial X_j} P_{ij}^{\mathrm{M}}\, \mathrm{d}\Omega_0 + f_{iI}^{HG} \tag{42}$$

For a one-point quadrature element, the above can be written as

$$f_{iI}^{\mathrm{int}} = A_e B_{jI}^{\mathrm{T}}(\mathbf{0}) P_{ji}^{\mathrm{M}} + f_{iI}^{HG} \tag{43}$$

where A_e is the area of element e, and $\mathbf{B}(\mathbf{0})$ and $\mathbf{f}^{HG}$ are defined, respectively, as:

$$B_{jI}(\mathbf{0}) = \frac{\partial \Psi_I(\mathbf{0})}{\partial X_j} \tag{44}$$

$$f_{iI}^{HG} = A_e Q_i \gamma_I \tag{45}$$

For an element that is cut by a crack, the integration method proposed in Song *et al.* [29] is used.

7. STABILITY OF MACROMATERIAL

The issue of the ellipticity of the macromodel is more intricate than for the linkage involving only the linear terms in (10). In fact, it becomes impossible to show the ellipticity of the macrometerial

DOI: 10.1002/nme

in the standard sense, although it is possible to show that the macroelement stiffness matrix is positive definite.

In order to examine this in more detail, we will first examine the consequences of convexity within the perforated unit cell on the ellipticity of the macromaterial. We will then show that convexity of the material in the perforated unit cell implies the positive definiteness of the tangent stiffness for the stabilized one-point quadrature element used for the macromodel. This insures that the discrete problem for the bulk material is stable.

We first note that convexity of the micromaterial and macromaterial requires, respectively, that

$$\dot{\mathbf{F}}:\mathbf{C}^{\mathrm{m}}:\dot{\mathbf{F}}>0 \quad \forall\dot{\mathbf{F}} \tag{46}$$

$$\dot{\mathbf{F}}:\mathbf{C}^{\mathrm{M}}:\dot{\mathbf{F}}>0 \quad \forall\dot{\mathbf{F}} \tag{47}$$

where $\mathbf{C}^{\mathrm{m}}$ and $\mathbf{C}^{\mathrm{M}}$ are tangent material matrices of that, respectively, relate $\dot{\mathbf{P}}$ to $\dot{\mathbf{F}}$ by

$$\dot{\mathbf{P}}^{\mathrm{m}}=\mathbf{C}^{\mathrm{m}}:\dot{\mathbf{F}}^{\mathrm{m}} \tag{48}$$

$$\dot{\mathbf{P}}^{\mathrm{M}}=\mathbf{C}^{\mathrm{M}}:\dot{\mathbf{F}}^{\mathrm{M}} \tag{49}$$

The rank-one stability condition, often called the ellipticity condition is

$$\mathbf{g}\otimes\mathbf{h}:\mathbf{C}^{\mathrm{M}}:\mathbf{g}\otimes\mathbf{h}>0 \quad \forall\mathbf{g} \text{ and } \mathbf{h} \tag{50}$$

The above condition is equivalent to the condition for the ellipticity of the governing PDE.

Then invoking the tangent material relation for the micromaterial (46), we have

$$\int_{\tilde{\Omega}_0^{\mathrm{m}}}\dot{\mathbf{F}}^{\mathrm{m}}:\mathbf{P}^{\mathrm{m}}\,\mathrm{d}\Omega=\int_{\tilde{\Omega}_0^{\mathrm{m}}}\dot{\mathbf{F}}^{\mathrm{m}}:\mathbf{C}^{\mathrm{m}}:\dot{\mathbf{F}}^{\mathrm{m}}\,\mathrm{d}\Omega>0 \tag{51}$$

where the inequality follows from the assumption that the material in the perforated unit cell is convex, i.e. it satisfies Equation (46). From the general form of the Hill–Mandel inequality and Equation (48), it follows then that

$$\dot{\mathbf{F}}^{\mathrm{M}}:\mathbf{P}^{\mathrm{M}}+\alpha\dot{\mathbf{q}}\cdot\dot{\mathbf{Q}}>0 \quad \forall\dot{\mathbf{F}}^{\mathrm{M}} \text{ and } \dot{\mathbf{q}} \tag{52}$$

where

$$\alpha=\begin{cases}0 & \text{for MAD method without hourglass multiscale coupling}\\ 1 & \text{for MAD method with hourglass multiscale coupling}\end{cases} \tag{53}$$

We note first that the above implies convexity at the macroscale if we do not consider the hourglass modes. In that case $\alpha=0$, and we have

$$\dot{\mathbf{F}}^{\mathrm{M}}:\dot{\mathbf{P}}^{\mathrm{M}}=\dot{\mathbf{F}}^{\mathrm{M}}:\mathbf{C}^{\mathrm{M}}:\dot{\mathbf{F}}^{\mathrm{M}}>0 \quad \forall\dot{\mathbf{F}}^{\mathrm{M}} \tag{54}$$

i.e. the convexity condition of the macromaterial.

This also implies the rank-one stability condition. To demonstrate this, we simply note that for any $\mathbf{g}$ and $\mathbf{h}$, we can let $\dot{\mathbf{F}}=\mathbf{g}\otimes\mathbf{h}$; hence, Equation (54) implies the rank-one stability condition.

However, neither convexity nor rank-one stability can be deduced if $\alpha=1$, i.e. for the method proposed here, since Equation (52) then does not imply Equation (54).

DOI: 10.1002/nme

Nevertheless, it can be shown that the tangent stiffness matric of the bulk material is positive definite. We assume that the generalized strain rates and stress rates are related by

$$\begin{Bmatrix} \dot{\mathbf{P}} \\ \dot{\mathbf{Q}} \end{Bmatrix} = \underbrace{\begin{bmatrix} \mathbf{C}^{\mathrm{M}} & \mathbf{C}_{\sigma\gamma}{}^{\mathrm{M}} \\ (\mathbf{C}_{\sigma\gamma}{}^{M})^{\mathrm{T}} & \mathbf{C}_{\gamma}^{\mathrm{M}} \end{bmatrix}}_{\bar{\mathbf{C}}^{\mathrm{M}}} \begin{Bmatrix} \dot{\mathbf{F}} \\ \dot{\mathbf{q}} \end{Bmatrix} \tag{55}$$

The macrotangent stiffness is given by

$$\mathbf{K}_e^{\mathrm{M}} = A_e [\mathbf{B}^{\mathrm{T}} \ \ \boldsymbol{\gamma}^{\mathrm{T}}] \bar{\mathbf{C}}^{\mathrm{M}} \begin{Bmatrix} \mathbf{B} \\ \boldsymbol{\gamma} \end{Bmatrix} \tag{56}$$

where A_e is the area of element e and $\mathbf{B}$ is the matrix defined in Equation (44). Note that these relations give both the material and geometric tangent stiffness, since $\bar{\mathbf{C}}^{\mathrm{M}}$ includes the initial stress; hence, they apply to arbitrary nonlinear problems.

We now wish to show that

$$\dot{\mathbf{d}}_e^{\mathrm{T}} \mathbf{K}_e^{\mathrm{M}} \dot{\mathbf{d}}_e^{\mathrm{T}} > 0 \quad \forall \dot{\mathbf{d}}_e \neq 0 \tag{57}$$

Substituting Equation (56) into Equation (57) and using Equations (36) and (44) give

$$\dot{\mathbf{d}}_e^{\mathrm{T}} \mathbf{K}_e^{\mathrm{M}} \dot{\mathbf{d}}_e^{\mathrm{T}} = A_e (\dot{\mathbf{F}}^{\mathrm{M}} : \dot{\mathbf{P}}^{\mathrm{M}} + \dot{\mathbf{q}} \cdot \dot{\mathbf{Q}}) > 0 \tag{58}$$

where the inequality follows from Equation (52). Thus, the bulk stiffness, which does not include the behavior of the macrocrack, is positive definite. We stress that only the bulk material tangent stiffness is positive definite. The combination of the stiffnesses of the cohesive law acting on the macrocrack and the bulk material stiffness is not positive definite.

As summarized by Marsden and Hughes [34], convexity in $\mathbf{F}$ is often considered as an unacceptable condition, because

1. it precludes buckling,
2. it is not frame invariant,
3. the behavior as $J \to 0$ is not reasonable.

We note that as already pointed out in Belytschko *et al.* [11], we are not concerned with problems involving buckling or those where $J \to 0$. The absence of frame invariance is more troubling. However, we emphasize that convexity is used only as a criterion to remove material from the RVE. Therefore, its undesirable properties may not invalidate its use.

8. IMPLEMENTATION

The governing equations were integrated by the central difference method. The loads were applied very slowly, so that dynamic effects were small during most of the simulation; the kinetic energy did not exceed 1% of the total energy. This approach bypasses some of difficulties associated with the snapback behavior on the equilibrium path.

DOI: 10.1002/nme

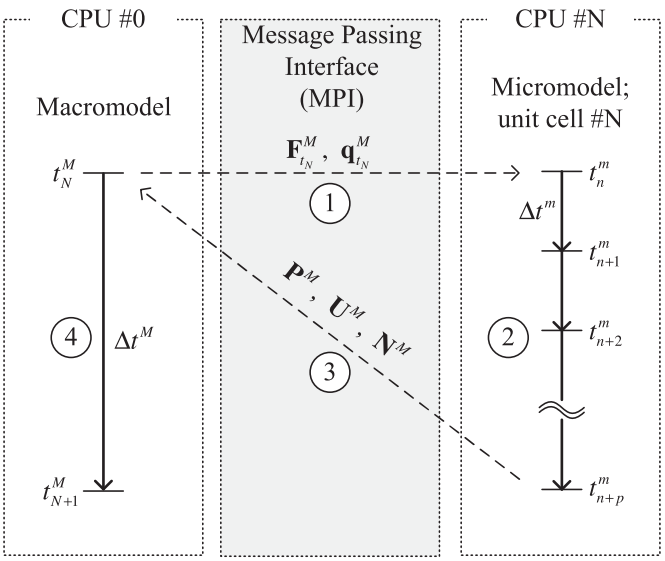

Figure 11. The macro–micro coupling scheme of the MAD method; the circled numbers indicate the sequence of the steps.

A schematic of the approach is shown in Figure 10. As shown, only a few of hot spots are linked with micromodels. Note that cells 3 and 4 contain strong discontinuities, thus, the coarse-grained failure information within those unit cells is provided to the associated elements in the macromodel. As shown in Figure 11, smaller time step was used for the micromodels.

The method was run on a parallel computer. A message passing interface module is used for the communication between the macromodel and the micromodels.

9. NUMERICAL EXAMPLES

The evaluation of a multiscale method for failure poses some challenges. Comparison with experimental results is usually inconclusive, since the material constants for failure are not readily available. We were not able to find experiments that provide both subscale properties and a macroscale response. Analytic results and manufactured solutions are also not available.

Therefore, we have chosen to use comparison with direct numerical simulation (DNS) to evaluate the method. In each cases, a detailed model with the target resolution over the entire model (or subdomain of interest) is considered the reference solution, i.e. the DNS. The multiscale solution is then compared with the DNS to evaluate its effectiveness.

In all examples, we consider a matrix–fiber composite material. The microstructure is shown in Figure 12. The macromodel is constructed by repeating the unit cells. The fiber/matrix volume fraction is 10%, and we then use the model as a unit cell for the computations. The material properties of the matrix and the fiber along with its homogenized material are shown in Table II; for the calculation of the homogenized material properties, we used a conventional homogenization theory.

DOI: 10.1002/nme

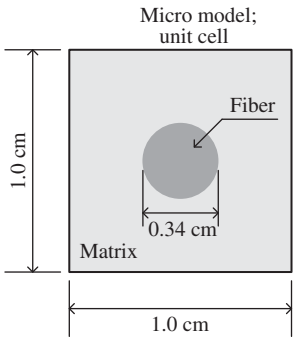

Figure 12. The unit cell of the matrix–fiber composite material used in the reported computations.

Table II. Material properties of the matrix–fiber composite material.

Material	Young's modulus (GPa)	Poisson ratio	Density (kg/m^3)
Matrix	67.5	0.36	2700.0
Fiber	413.0	0.20	2340.0
Homogenized material (10% of matrix–fiber fraction)	75.6	0.35	2500.0

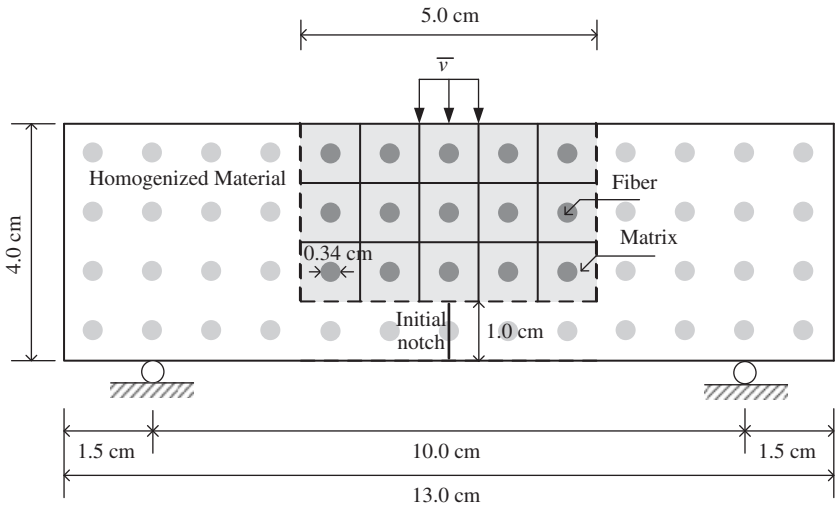

Figure 13. Initial setup for failure of composite beam due to three-point bending.

9.1. Three-point bending beam problem

As an application of the MAD method, we considered failure of a 13×4 cm composite beam subjected to three-point bending as shown in Figure 13. An initial notch is introduced at the bottom center of the beam; the crack propagation at the mid span mainly depends on mode I fracture.

DOI: 10.1002/nme

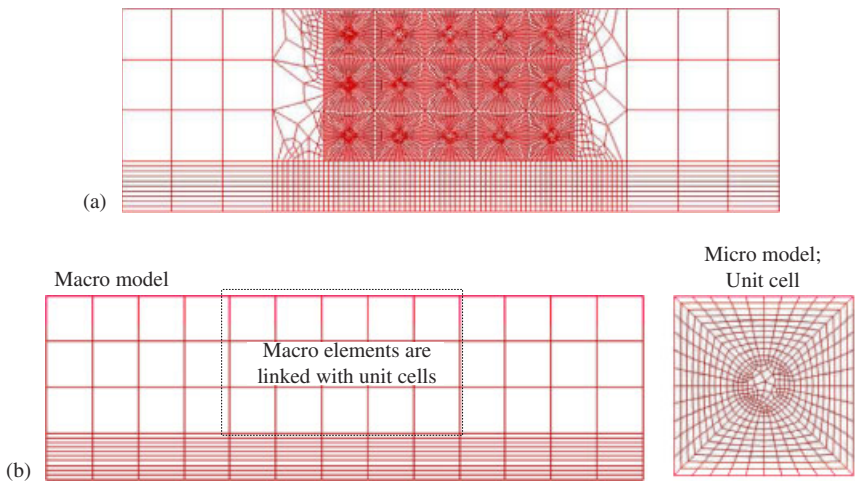

Figure 14. Finite element discretizations for: (a) the DNS and (b) the coarse model and a typical unit cell model for the MAD method; each cell is linked to an element of the macromodel.

For the DNS model, we discretized the beam with 9634 four-node quadrilateral elements as shown in Figure 14(a); the center of the beam is quite detailed and of the same resolution as the unit cells. For the multiscale solution, the entire beam was discretized with a coarse mesh, and the 5×3 elements at the center of the beam are linked to unit cells. Note that outside of the center area in both the DNS and MAD models, we considered a homogeneous material with an effective elastic modulus which is computed by conventional homogenization theory. The material properties are shown in Table II. We used a maximum principal tensile strain criterion for fracture with a fracture strain of 3.0%. A cohesive law was used at the fiber/matrix interface with a fracture energy of $G_f = 6.0 \times 10^4\,\mathrm{N/m}$.

Figures 15(a) and (b) show an intermediate stage of the crack propagation in the DNS model and the MAD model, respectively. As can be seen from Figure 15(a), the crack path in the DNS model is quite jagged due to the microstructures of the beam. In the MAD method, such jagged crack paths are straight within the elements; see Figure 15(b). This is the distinct feature of the coarse graining of the microcracks with the MAD method.

The adequacy of the multiscale solution can be judged from Figure 16, which compares the load–deflection curves for the MAD to that for the DNS. As can be seen from Figure 16, there are only some minor discrepancies due to the different dynamic response of the DNS and the MAD method. However, the overall responses are very similar, and the error in the prediction of the peak load is less than 1%.

This accuracy in the peak load is probably fortuitous, since the error in the load is much greater along other parts of the load–deflection curve.

9.2. Four-point bending beam problem

As an application of the MAD method to the analysis for a curved crack, we consider a four-point bending problem. The problem definition is shown in Figure 17. Figure 18(a) shows the DNS model, the microstructure in the center of the beam is quite detailed and requires thousand of elements for its resolution. Figure 18(b) shows the result for DNS: note the jagged and curved

DOI: 10.1002/nme

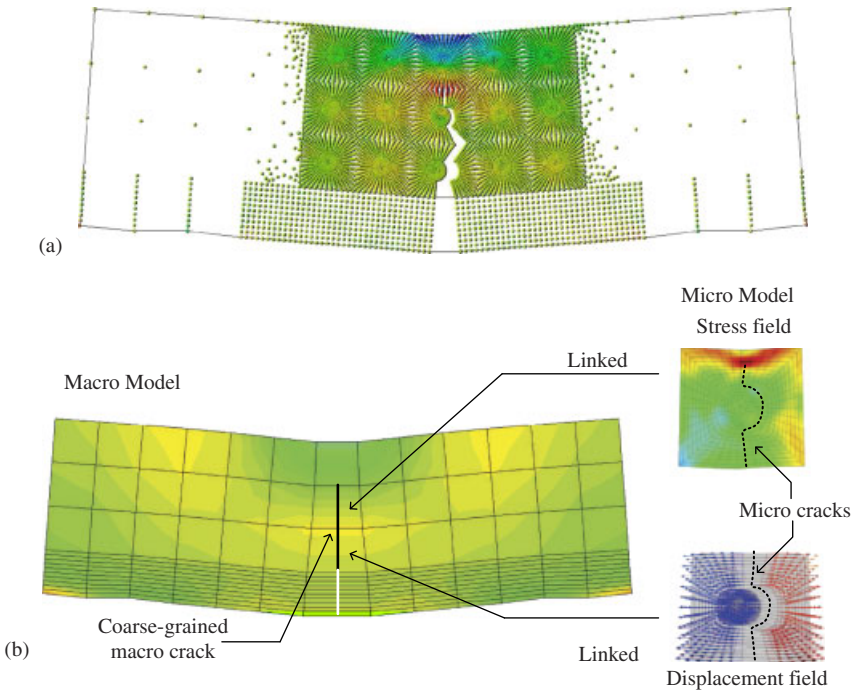

Figure 15. The plots of σ_{xx} contour for: (a) the DNS and (b) the MAD method; the deformations are magnified by factor of two.

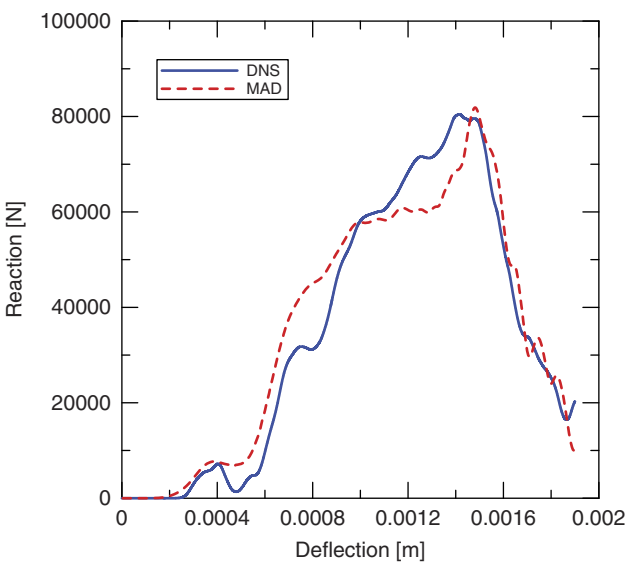

Figure 16. Comparison of load–deflection curves for the failure of the composite beam for the three-point bending beam problem.

DOI: 10.1002/nme

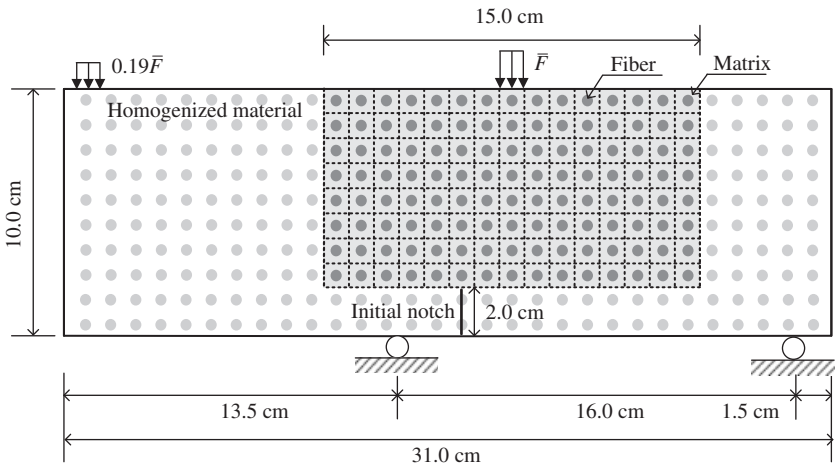

Figure 17. Initial setup for failure of composite beam due to four-point bending.

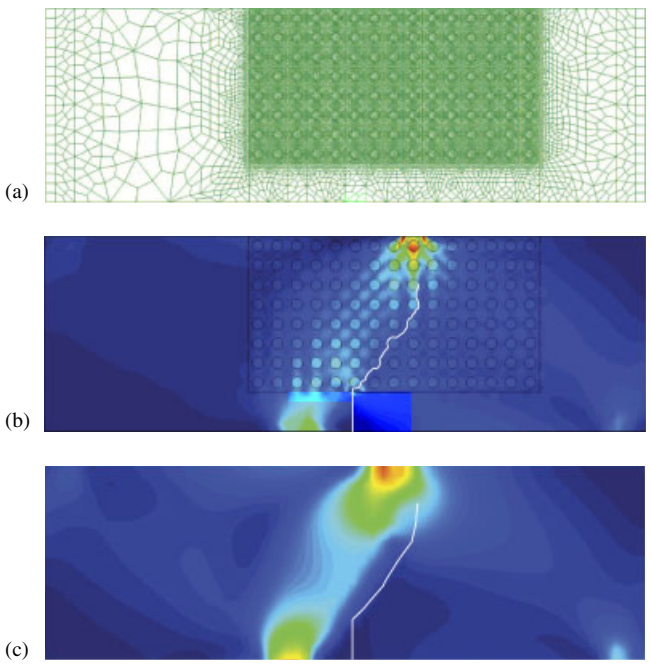

Figure 18. Four-point bending beam problem: (a) finite element discretizations for the DNS; (b) the plots of effective stress contour for the DNS; and (c) the plots of effective stress contour for the MAD method.

crack path that has progressed from the bottom to the top of the beam. Figure 18(c) shows the multiscale solution by the MAD method. The crack path is less jagged than that of DNS, but the overall crack path compares well with the DNS, and progresses the same distance.

DOI: 10.1002/nme

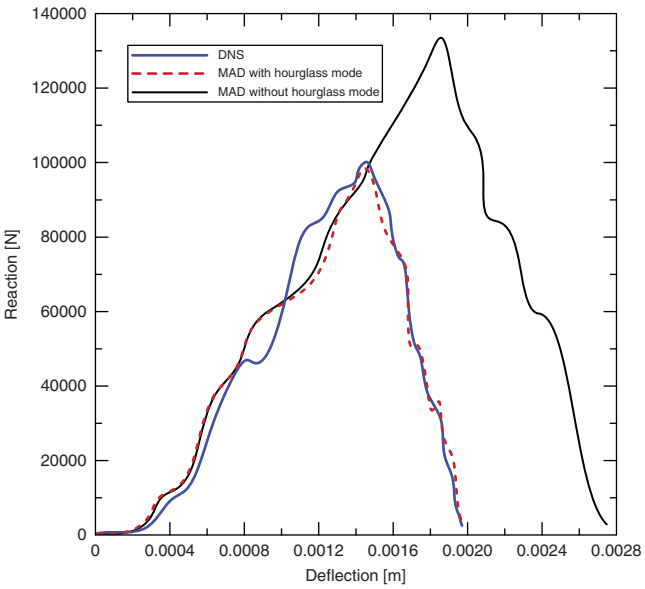

Figure 19. Comparison of load–deflection curves between the DNS and the MAD for the four-point bending beam problem.

The adequacy of the MAD method can be judged from Figure 19, which compares the load–deflection curves for the MAD to that for the DNS result. As can be seen from Figure 19, the error in the peak load is less than 1%; there are only some minor discrepancies in the final stages of the response.

10. CONCLUSIONS

An improved version of the MAD method, a multiscale method for failure analysis, has been presented. This improvement consists of adding an 'hourglass mode' to the prescribed displacements of a unit cell. This appears to be particularly advantageous when a unit cell fails by progression of a crack from one edge to the other, which is often the case.

In the MAD method, the microcracking at finer scales is represented by an aggregate, equivalent crack at the coarse scale. We have shown that the formula for extracting the magnitude and the normal to the equivalent discontinuity at the macroscale is not changed by the addition of the hourglass mode. However, additional generalized stresses and strains are needed at the macroscale. In this paper, we have treated these additional generalized stresses as hourglass forces in the four-node quadrilateral. These can also be incorporated into other elements by adding the bilinear term to the displacement field through meshfree approximations. Another approach we are considering for treating this mode is a micropolar continuum. However, using classical continuum mechanics for the macroscale bestows significant benefits; hence, we are inclined to continuing our current

DOI: 10.1002/nme

approach. As for the original MAD method, the noteworthy features of this improved method are:

1. the decomposition of the unit cells into subdomains where the material is convex or not, i.e. the construction of perforated unit cells,
2. the extraction of a single coarse-grained macrodiscontinuity from the unstable behavior of the unit cell.

In the absence of the hourglass mode, the above leads to problems that are elliptic and hence well posed. By adding the hourglass mode, this property is lost, although the bulk stiffness is still positive definite.

The proposed methodology still requires a considerable amount of research. The mixed boundary conditions described here for when the crack breaks the surface are relatively *ad hoc*, although they appear to be effective. This issue, the scaling of the unit cell, and the stability issues all require further investigation.

ACKNOWLEDGEMENTS

The support of the Army Office of Scientific Research under Grant W911-NF-08-1-0212, and the Office of Naval Research under Grants N00014-08-1-1191 and N00014-06-1-0380 are gratefully acknowledged.

REFERENCES

1. Zohdi TI, Wriggers P. *Introduction to Computational Micromechanics*. Lecture Notes in Applied and Computational Mechanics, vol. 20. Springer: Berlin, 2005.
2. Rudnicki JW, Rice JR. Conditions for the localization of deformation in pressure-senstive dilatant materials. *Journal of the Mechanics and Physics of Solids* 1975; **23**:371–394.
3. Belytschko T, Liu WK, Moran B. *Nonlinear Finite Elements for Continua and Structures*. Wiley: New York, 2000.
4. Bažant ZP, Belytschko T. Wave-propagation in a strain-softening bar: exact solution. *Journal of Engineering Mechanics* (ASCE) 1985; **111**(3):381–389.
5. Bažant ZP, Belytschko T, Chang TP. Continuum theory for strain-softening. *Journal of Engineering Mechanics* (ASCE) 1984; **110**(12):1666–1692.
6. Lasry D, Belytschko T. Localization limiters in transient problems. *International Journal of Solids and Structures* 1988; **24**(6):581–597.
7. Kouznetsova V, Geers MGD, Brekelmans WAM. Multi-scale constitutive modelling of heterogeneous materials with a gradient-enhanced computational homogenization scheme. *International Journal for Numerical Methods in Engineering* 2002; **54**:1235–1260.
8. Vernerey FJ, Liu WK, Moran B. Multi-scale micromorphic theory for hierarchical materials. *Journal of the Mechanics and Physics of Solids* 2007; **55**:2603–2651.
9. Fish J, Yuan Z. Multiscale enrichment based on partition of unity. *International Journal for Numerical Methods in Engineering* 2005; **62**:1341–1359.
10. Oskay C, Fish J. Eigendeformation-based reduced order homogenization for failure analysis of heterogeneous materials. *Computer Methods in Applied Mechanics and Engineering* 2007; **196**:1216–1243.
11. Belytschko T, Loehnert S, Song JH. Multiscale aggregating discontinuities: a method for circumventing loss of material stability. *International Journal for Numerical Methods in Engineering* 2008; **73**:869–894.
12. Belytschko T, Black T. Elastic crack growth in finite elements with minimal remeshing. *International Journal for Numerical Methods in Engineering* 1999; **45**(5):601–620.
13. Moës N, Dolbow J, Belytschko T. A finite element method for crack growth without remeshing. *International Journal for Numerical Methods in Engineering* 1999; **46**(1):131–150.
14. Massart TJ, Peerlings RHJ, Geers MGD. An enhanced multi-scale approach for masonry wall computations with localization of damage. *International Journal for Numerical Methods in Engineering* 2007; **69**:1022–1059.

DOI: 10.1002/nme

15. Nemat-Nasser S, Hori M. *Micromechanics*: *Overall Properties of Heterogeneous Solids* (2nd edn). Elsevier: Amsterdam, New York, 1999.
16. Belytschko T, Gracie R, Xu M. Concurrent coupling of atomistic and continuum models. In *Multiscale Methods Bridging the Scales in Science and Engineering*, Fish J (ed.). Oxford Press: Oxford, 2009.
17. Guidault PA, Allix O, Champaney L, Navarro JP. A two-scale approach with homogenization for the computation of cracked structures. *Computers and Structures* 2007; **85**:1360–1371.
18. Ibrahimbegovic A, Markovic D. Strong coupling methods in multi-phase and multi-scale modeling of inelastic behavior of heterogeneous structures. *Computer Methods in Applied Mechanics and Engineering* 2003; **192**: 3089–3107.
19. Abraham FF, Broughton JQ, Bernstein N, Kaxiras E. Spanning the continuum to quantum length scales in a dynamic simulation of brittle fracture. *Europhysics Letters* 1998; **44**:783–787.
20. Khare R, Mielke SL, Paci JT, Zhang SL, Ballarini R, Schatz GC, Belytschko T. Coupled quantum mechanical/molecular mechanical modeling of the fracture of defective carbon nanotubes and graphene sheets. *Physical Review B* 2007; **75**. Art. No. 075412.
21. Xiao SP, Belytschko T. A bridging domain method for coupling continua with molecular dynamics. *Computer Methods in Applied Mechanics and Engineering* 2004; **193**:1645–1669.
22. Wagner GJ, Liu WK. Coupling of atomistic and continuum simulations using a bridging scale decomposition. *Journal of Computational Physics* 2003; **190**:249–274.
23. Curtin WA, Miller RE. Atomistic/continuum coupling in computational material science. *Modelling and Simulation in Material Science and Engineering* 2003; **11**:R33–R68.
24. Feyel F, Chaboche JL. FE^2 multiscale approach for modelling the elastoviscoplastic behaviour of long fiber SiC/Ti composite materials. *Computer Methods in Applied Mechanics and Engineering* 2000; **183**:309–330.
25. Feyel F. A multilevel finite element method (FE^2) to describe the response of highly non-linear structures using generalized continua. *Computer Methods in Applied Mechanics and Engineering* 2003; **192**:3233–3244.
26. Flanagan DP, Belytschko T. A uniform strain hexahedron and quadrilateral with orthogonal hourglass control. *International Journal for Numerical Methods in Engineering* 1981; **17**:679–706.
27. Belytschko T, Bachrach WE. Efficient implementation of quadrilaterals with high coarse-mesh accuracy. *Computer Methods in Applied Mechanics and Engineering* 1986; **54**:279–301.
28. Loehnert S. Computational homogenization of microheterogeneous materials at finite strains including damage. *Ph.D. Thesis*, University Hannover, Germany, 2004.
29. Song JH, Areias PMA, Belytschko T. A method for dynamic crack and shear band propagation with phantom nodes. *International Journal for Numerical Methods in Engineering* 2006; **67**:868–893.
30. Fish J. The *s*-version of the finite element method. *Computers and Structures* 1992; **43**(3):539–547.
31. Fish J, Guttal R. The *s*-version of finite element method for laminated composites. *International Journal for Numerical Methods in Engineering* 1996; **39**:3641–3662.
32. Rabczuk T, Belytschko T. Cracking particles: a simplified meshfree method for arbitray evolving cracks. *International Journal for Numerical Methods in Engineering* 2004; **61**:2316–2343.
33. Bellec J, Dolbow JE. A note on enrichment functions for modelling crack nucleation. *Communications in Numerical Methods in Engineering* 2003; **19**:921–932.
34. Marsden JE, Hughes TJ. *Mathematical Foundations of Elasticity*. Dover Publications: New York, 1994.

DOI: 10.1002/nme